Southern Ocean CO2 sink: The contribution of the sea ice

Bruno Delille, Martin Vancoppenolle, Nicolas-Xavier Geilfus, Bronte Tilbrook, Delphine Lannuzel, Véronique Schoemann, Sylvie Becquevort, Gauthier Carnat, Daniel Delille, Christiane Lancelot, et al.

AGU PUBLICATIONS

JGR

Journal of Geophysical Research: Oceans

RESEARCH ARTICLE

10.1002/2014JC009941

Key Points:
- Antarctic sea ice act as a significant sink for atmospheric CO_2 in spring and summer
- Significance of main sea ice processes on CO_2 concentration are assessed and discussed
- In situ measurements were up scaled with the NIMO-LIM3 model

Correspondence to:
Bruno Delille,
Bruno.Delille@ulg.ac.be

Citation:
Delille, B., et al. (2014), Southern Ocean CO_2 sink: The contribution of the sea ice, *J. Geophys. Res. Oceans*, *119*, 6340–6355, doi:10.1002/2014JC009941.

Received 3 MAR 2014
Accepted 14 AUG 2014
Accepted article online 19 AUG 2014
Published online 22 SEP 2014

Southern Ocean CO_2 sink: The contribution of the sea ice

Bruno Delille[1], Martin Vancoppenolle[2], Nicolas-Xavier Geilfus[3], Bronte Tilbrook[4], Delphine Lannuzel[5,6], Véronique Schoemann[7], Sylvie Becquevort[8], Gauthier Carnat[7], Daniel Delille[9], Christiane Lancelot[7], Lei Chou[10], Gerhard S. Dieckmann[11], and Jean-Louis Tison[7]

[1]Unité d'Océanographie Chimique, MARE, Université de Liège, Liège, Belgium, [2]Laboratoire d'Océanographie et du Climat/Institut Pierre-Simon Laplace, CNRS/IRD/UPMC/MNHN, Paris, France, [3]Arctic Research Centre, Aarhus University, Aarhus, Denmark, [4]CSIRO Wealth from Oceans National Research Flagship and Antarctic Climate and Ecosystem Cooperative Research Centre, Hobart, Tasmania, Australia, [5]Antarctic Climate and Ecosystems Cooperative Research Centre, University of Tasmania, Hobart, Tasmania, Australia, [6]Institute for Marine and Antarctic Studies, University of Tasmania, Hobart, Tasmania, Australia, [7]Glaciology Unit, Department of Earth and Environmental Science, Université Libre de Bruxelles, Bruxelles, Belgium, [8]Ecologie des Systèmes Aquatiques, Université Libre de Bruxelles, Bruxelles, Belgium, [9]Observatoire Océanologique de Banyuls, Université P. et M. Curie, Banyuls sur mer, France, [10]Laboratoire d'Océanographie Chimique et Géochimie des eaux, Université Libre de Bruxelles, Bruxelles, Belgium, [11]Alfred-Wegener-Institut fuer Polar- und Meeresforschung, Bremerhaven, Germany

Abstract We report first direct measurements of the partial pressure of CO_2 (pCO_2) within Antarctic pack sea ice brines and related CO_2 fluxes across the air-ice interface. From late winter to summer, brines encased in the ice change from a CO_2 large oversaturation, relative to the atmosphere, to a marked undersaturation while the underlying oceanic waters remains slightly oversaturated. The decrease from winter to summer of pCO_2 in the brines is driven by dilution with melting ice, dissolution of carbonate crystals, and net primary production. As the ice warms, its permeability increases, allowing CO_2 transfer at the air-sea ice interface. The sea ice changes from a transient source to a sink for atmospheric CO_2. We upscale these observations to the whole Antarctic sea ice cover using the NEMO-LIM3 large-scale sea ice-ocean and provide first estimates of spring and summer CO_2 uptake from the atmosphere by Antarctic sea ice. Over the spring-summer period, the Antarctic sea ice cover is a net sink of atmospheric CO_2 of 0.029 Pg C, about 58% of the estimated annual uptake from the Southern Ocean. Sea ice then contributes significantly to the sink of CO_2 of the Southern Ocean.

1. Introduction

Climate models often consider sea ice is an inert barrier preventing air-sea exchange of gases, a concept which is presently challenged by observation and theoretical considerations. For decades, sea ice has been assumed to be an impermeable and inert barrier to air-sea exchange of CO_2 so that current assessment of global air-sea CO_2 fluxes or climate models does not include CO_2 exchanges over ice covered waters [*Takahashi et al.*, 2009; *Tison et al.*, 2002].

This paradigm relies on the CO_2 budgets of the water masses of the Weddell Sea. They suggest limited air-sea exchange of CO_2 in the Winter Surface Water when it is subducted and mixed with other water masses to form Weddell Bottom Water [*Poisson and Chen*, 1987; *Weiss*, 1987], a major contributor of Antarctic Bottom Water. However, *Gosink et al.* [1976] showed that sea ice is a highly permeable medium for gases based on work to estimate permeation constants of SF_6 and CO_2 within sea ice. These authors suggested that gas migration through sea ice could be an important factor in winter ocean-atmosphere exchange when the snow-ice interface temperature is above $-10^{\circ}C$. Fluxes of CO_2 over sea ice have been reported in the Arctic Ocean [*Geilfus et al.*, 2012, 2013; *Miller et al.*, 2011; *Nomura et al.*, 2010, 2013; *Papakyriakou and Miller*, 2011; *Semiletov et al.*, 2004, 2007] and in the Southern Ocean [*Zemmelink et al.*, 2006].

During sea ice growth, most of the impurities (gases, dissolved and particulate matter) are expelled from the pure ice crystals at the ice-water interface (skeletal layer). However, a small fraction of impurities (~10%) remains trapped in gaseous and liquid brine inclusions. These contribute to the overall sea ice porosity and host active auto and heterotrophic microbial communities [*Arrigo*, 2003; *Arrigo et al.*, 1997; *Lizotte*, 2001;

Thomas and Dieckmann, 2002]. Further removal of impurities occurs via brine drainage processes (gravity drainage and flushing) and convection that are mainly controlled by the history of the thermal regime of the ice [*Eicken*, 2003; *Notz and Worster*, 2009; *Weeks and Ackley*, 1986; *Wettlaufer et al*., 1997].

Brine volume and salinity adjust to temperature changes in order to maintain thermal equilibrium within the ice [*Cox and Weeks*, 1983]. A 5% relative brine volume is a theoretical threshold above which sea ice permeability for liquid increases drastically [*Golden et al*., 1998]. It is also likely to represent a threshold above which air-ice gas exchange increases [*Buckley and Trodahl*, 1987], although *Zhou et al*. [2013] suggest higher threshold (between 7.5 and 10%). This permeability threshold would occur at a temperature of −10°C for a bulk ice salinity of 10, corroborating the observation that sea ice is a highly permeable medium for gases [*Gosink et al*., 1976] allowing air-ice gas exchanges.

The aim of this study is to describe observed pCO_2 and CO_2 fluxes relationships to sea ice temperature from various locations around Antarctica. We assess and compare the relative contribution of biotic and abiotic processes to the observed changes of pCO_2 and estimated related uptake of atmospheric CO_2. Finally, we provide a first estimate of Antarctic sea ice contribution to CO_2 exchanges with the atmosphere using two independent methods: (a) a global estimate derived from the relative importance of each process controlling the sea ice brine pCO_2 and (b) integrating the observed sea ice temperature versus CO_2 fluxes relationship into a sea ice 3-D-model.

2. Material and Methods

2.1. Sampling Strategy

Measurements were carried out during the 2003/V1 cruise on the *R.V. Aurora Australis* from 27 September 2003 to 20 October 2003 in the Indian sector of the Southern Ocean (63.9–65.3°S, 109.4–117.7°E), the ISPOL (Ice Station Polarstern) drift station experiment onboard the *R.V. Polarstern* from 29 November 2004 to 31 December 2005 in the Weddell Sea (67.35–68.43°S, 55.40–54.57°W), and the SIMBA (Sea Ice Mass Balance in the Antarctica) drift station experiment onboard the *R.V. Nathaniel B. Palmer* from 1 October 2007 to 23 October 2007 in the Bellingshausen Sea (69.51–70.45°S, 94.59–92.30°W). A complete description of these different working stations could be found in *Massom et al*. [2006] for V1, in *Tison et al*. [2008] for ISPOL, and in *Lewis et al*. [2011] for SIMBA. Only first year pack ice was investigated during 2003/V1 and SIMBA cruises, while both first year and multiyear pack ice were sampled during ISPOL experiment. Sampling was only carried out in floes without melt ponds or slush surface layers.

2.2. pCO_2 of Brines

Sampling of ice brine was conducted by drilling shallow sackholes (ranging from 15 cm down to almost full ice thickness) through the surface of the ice sheet. The brine from adjacent brine channels and pockets was allowed to seep into the sackhole for 30–60 min, with the hole covered with a plastic lid [*Gleitz et al*., 1995], reportedly the best current method to sample brines for chemical studies [*Papadimitriou et al*., 2004]. Brines was pumped from the hole using a peristaltic pump (Masterflex® - Environmental Sampler), supplied to the device for measurements of partial pressure of CO_2 (pCO_2), and recycled back at the bottom of the sackhole. The latter were carried out using a membrane contractor equilibrator (Membrana® Liqui-cell) coupled to an infrared gas analyzer (IRGA, Li-Cor® 6262). Seawater or brines flowed into the equilibrator at a maximum rate of 1 L min^{-1} and a closed air loop ensured circulation through the equilibrator and the IRGA at a rate of 3 L min^{-1}. Temperature was measured simultaneously in situ and at the outlet of the equilibrator using Li-Cor® sensors. Temperature correction of pCO_2 was applied assuming that the relation from *Copin-Montégut* [1988] is valid at low temperature and high salinity. The IRGA was calibrated soon after returning to the ship while the analyzer was still cold. For V3/2001, CO_2-in-air standards calibrated on the World Meteorological Organisation X-85 molar scale (mixing ratios of 304.60, 324.65, and 380.03 ppm) were supplied by Commonwealth Scientific and Industrial Research Organisation (CSIRO) Atmospheric Research, Australia. CO_2-in-air standards with mixing ratios of 0 ppm and 350 ppm of CO_2 were supplied by Air Liquide Belgium® for the ISPOL and SIMBA cruise. Stable field pCO_2 readings usually occurred within 3 min of flowing gas into the IRGA. The equilibration system ran 6 min before averaging the values given by the IRGA and temperature sensors over 30 s and recording the averaged values with a data logger (Li-Cor® Li-1400). All the devices (except the peristaltic pump) were enclosed in an insulated box containing a 12 V power source and was warmed to keep the inside temperature just above 0°C.

2.3. Dissolved Inorganic Carbon and Total Alkalinity

A peristaltic pump (Masterflex® - Environmental Sampler) was used to collect brines from sackholes but also underlying water at the ice-water interface, 30 m deep and at an intermediate depth (5 m during 2003/V1 cruise and 1 m during ISPOL cruise) for dissolved inorganic carbon (DIC) and total alkalinity (TA) measurements.

DIC measurements on 2003/V1 were made using a single operator multiparameter metabolic analyzer (SOMMA) and UIC® 5011 coulometer [*Johnson et al*., 1998]. The system was calibrated by injecting known amounts of pure CO_2 into the system. The number of moles of pure CO_2 injected bracketed the amounts measured in sea ice brines and showed the measurement calibration did not change over the range of concentrations measured. The measurement precision and accuracy was checked during the analyses using certified reference materials provided by Dr. A. Dickson, Scripps Institution of Oceanography. Repeat analyses showed an accuracy and precision for the DIC measurements better than $\pm 0.1\%$.

TA was computed from pCO_2 and DIC using the CO_2 dissociation constants of *Mehrbach et al*. [1973] refitted by *Dickson and Millero* [1987]. We assumed a conservative behavior of dissociation constants during seawater freezing. During the ISPOL experiment, TA was measured using the classical Gran potentiometric method [*Gran*, 1952] on 100 mL GF/C filtered samples, with a reproducibility of $\pm 3\ \mu mol\ kg^{-1}$. DIC was computed from TA and pCO_2 for ISPOL.

2.4. Air-Ice CO_2 Fluxes

A chamber was used to measure air-ice CO_2 fluxes. The accumulation chamber (West system®) is a metal cylinder closed at the top (internal diameter 20 cm; internal height 9.7 cm) with a pressure compensation device. A rubber seal surrounded by a serrated-edge iron ring ensured an airtight connection between the base of the chamber and the ice. For measurement over snow, an iron cylinder was mounted at the base of the chamber to enclose snow down to the ice and prevent lateral advection of air through the snow. The chamber was connected in a closed loop between the air pump ($3\ L\ min^{-1}$) and the IRGA. The measurement of pCO_2 in the chamber was recorded every 30 s for at least 5 min. The flux was computed from the slope of the linear regression of pCO_2 against time ($r^2 \geq \pm\ 0.99$) according to *Frankignoulle* [1988]. The uncertainty of the flux computation due to the standard error on the regression slope is on average $\pm 3\%$.

2.5. Air-Ice CO_2 Flux/Ice Temperature Relationship

Using field data, we calculated a relationship between CO_2 fluxes (F_{CO2}) over both first year and multiyear ice as a function of sea ice temperature (T_{si}) at 5 cm depth (Figure 1a). The regression is composed of two second-order polynomial regressions valid between $-9°C$ and $-7°C$ and between $-7°C$ and $0°C$, respectively (Table 1).

2.6. Description of the Sea Ice Model

We used NEMO-LIM3 [*Madec*, 2008; *Vancoppenolle et al*., 2008] ocean-sea ice model to scale in situ measurements. NEMO (Nucleus for European Modelling of the Ocean) is a widely used ocean model, while LIM3 (Louvain-la-Neuve Ice Model) is an advanced large-scale sea ice model, carefully validated for both hemispheres. LIM3 is a C-grid dynamic thermodynamic model, including the representation of the subgrid-scale distributions of ice thickness, enthalpy, and salinity as well as snow volume. Ice dynamics are resolved using an elasto-visco-plastic rheology, following concepts of *Hunke and Dukowicz* [1997]. Snow and sea ice thermodynamics include vertical diffusion of heat with a formulation of brine thermal effect. There is also an explicit formulation of brine entrapment and drainage. Sources and sinks of ice mass include basal growth and melt, surface melt, new ice formation in open water, as well as snow-ice formation. In order to account for subgrid-scale variations in ice thickness, ice volume and area are split into five categories of ice thickness. Thermodynamic (ice growth and melt) as well as dynamical (rafting and ridging) processes control the redistribution of ice state variables within the ice thickness categories. LIM3 is coupled to NEMO, a hydrostatic, primitive equation finite difference ocean model running on a $2° \times 2° \cos \phi$ grid called ORCA2.

We used the NEMO-LIM3 model output rather than satellite derivations of sea ice temperature as the latter are presently not reliable in all conditions [*Lewis*, 2010]. In comparison, we have reasonable confidence in the ice thickness, snow depth, and temperature simulated by LIM3, for the two following reasons. First, a series of one-dimensional validations of the thermodynamic component of LIM3 was made over various sites in both hemispheres [*Vancoppenolle et al*., 2007]. Vertical profiles of temperature, salinity, as well as ice

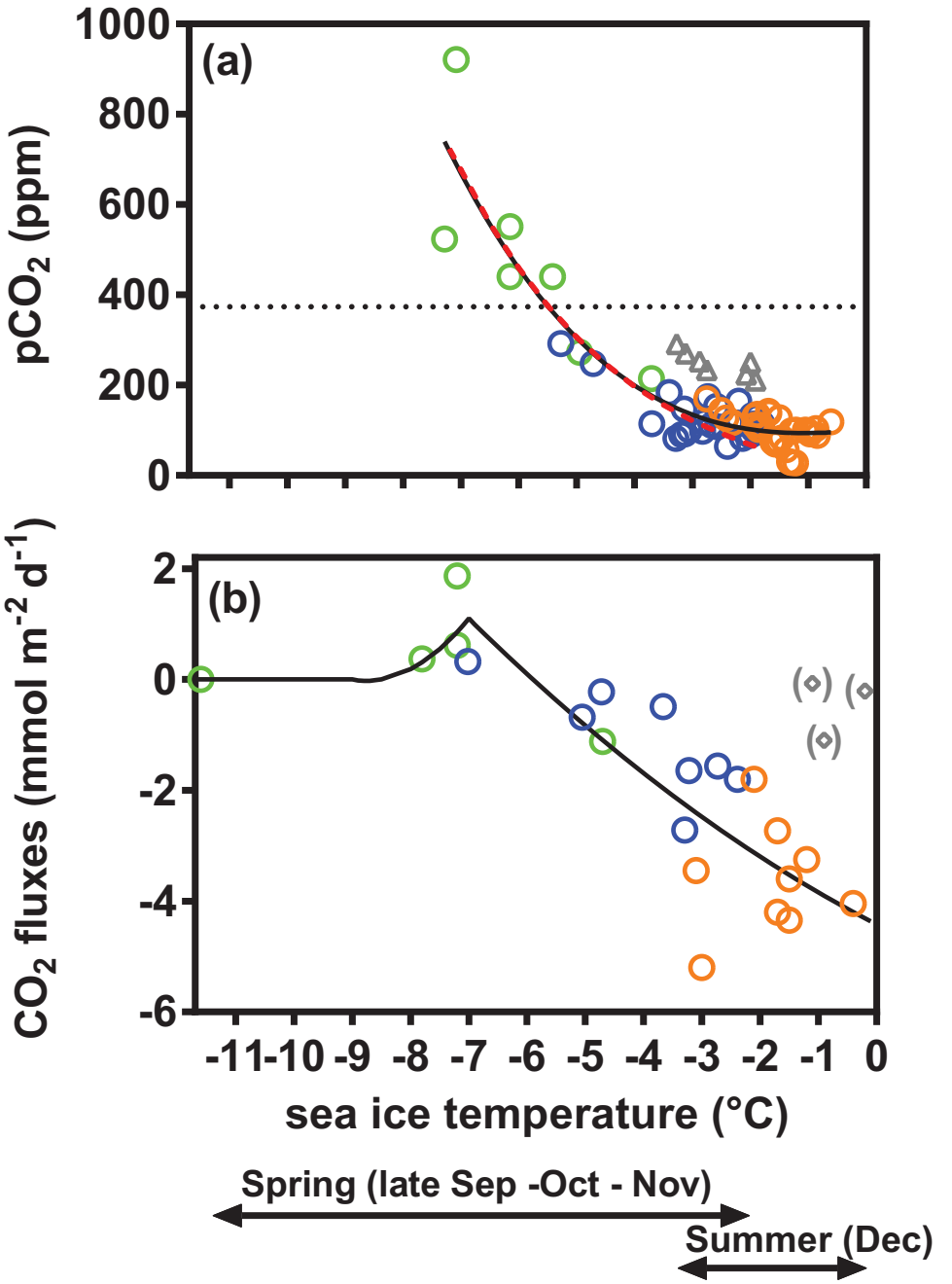

Figure 1. (a) pCO_2 within brines ($pCO_{2\ brines}$) versus sea ice temperature integrated over the depth of sackholes (green: 2003/V1cruise, orange: ISPOL cruise, and blue: SIMBA cruise). Gray triangles correspond to two stations carried out on a snow-loaded floe which experienced flooding. Horizontal dotted line and solid curve are pCO_{2air} and the regressed $pCO_{2\ brine}$, respectively. Fit expression of the regressed pCO_2 brine as a function of sea ice temperature (T_{si}) is $pCO_{2\ brine} = 101.5 + 12.96\ T_{si} + 3.915\ T_{si}^2 - 1.360\ T_{si}^3$ (number of points analyzed and coefficient of determination are 65 and 0.8625, respectively). Red dashed curve represents the theoretical variation related to both dilution and the thermodynamic effect of temperature increase (see text for details). (b) Net air-sea ice CO_2 fluxes versus snow-ice interface temperature. Solid curve represents the relationship of air-ice CO_2 fluxes to snow-ice interface temperature used for reconstructing air-ice CO_2 fluxes from the NEMO-LIM3 model. Flux measurements during superimposed ice events (gray diamonds) were excluded from the calculation. Correspondence between season and ice temperature is only indicative and corresponds to the conditions encountered during our surveys.

thickness and snow depth were found to be in close agreement with field observations. In particular, the sea ice permeability transitions seem to be quite well captured. Second, an extensive large-scale validation of LIM3, forced by NCEP-NCAR daily reanalyses of meteorological data [*Kalnay et al.*, 1996] was performed

Table 1. Fit Expression of the Relationship Between CO_2 Fluxes (F_{CO2}) Over Both First Year and Multiyear Ice as a Function of Sea Ice Temperature (T_{si}) at 5 cm Depth Used for Reconstructing Air-Ice CO_2 Fluxes From the NEMO-LIM3 Model as It Appears in Figure 1b (Solid Curve)[a]

T_{si} (°C)	F_{CO2} (mmol C m^{-2} d^{-1})
$T_{si} < -9$	0
$-9 < T_{si} < -7$	$F_{CO2} = 27.945 + 6.39\ T_{si} + 0.365\ T_{si}^2$
$T_{si} > -7$	$F_{CO2} = -4.41962 - 0.54286\ T_{si} + 0.035\ T_{si}^2$

[a]Number of samples, mean error, standard error, root-mean-square error, and coefficient of determination were 21, −0.099 mmol C m^{-2} d^{-1}, 0.995 mmol C m^{-2} d^{-1}, 0.953, and 0.728, respectively.

[*Vancoppenolle et al.*, 2008]. In the Antarctic, the simulated sea ice concentration, thickness, drift and salinity and snow depth model fields are in reasonable agreement with available observations. Because of errors in the wind forcing, there is a low bias in ice thickness along the east side of the Antarctic Peninsula, but this region is not of particular importance for the present analysis.

2.7. Computation of the Snow-Ice Interface Temperature and Air-Ice CO_2 Flux in the Sea Ice Model

In LIM3 (Figure 2), for each model grid cell, the sea ice thickness categories have a relative coverage a^l ($l = 1, \ldots, 5$). In each thickness category l, the sea ice is treated as a horizontally uniform column with ice thickness h_i^l and snow depth h_s^l. In order to compute the vertical temperature profile, the sea ice in each category is vertically divided into one layer of snow, with a midpoint temperature T_s and $N = 5$ layers of sea ice with midpoint temperatures T_i^{kl} ($k = 1, \ldots, 5$). The snow and sea ice temperatures are computed by the model by solving the heat diffusion equation. For the purpose of the present study, we diagnose the ice-air interfacial temperature by assuming the continuity of the heat conduction flux at the snow-ice interface:

$$T_{si} = \frac{k_i^1 T_i^1 h_s + k_s T_s h_i / N}{k_i^1 h_s + k_s h_i / N}, \quad (1)$$

where k_i^1 and k_s are the thermal conductivities of the first sea ice layer and of snow, respectively. The latter is done for each sea ice thickness category, which gives T_{si}^l ($l = 1, \ldots, 5$).

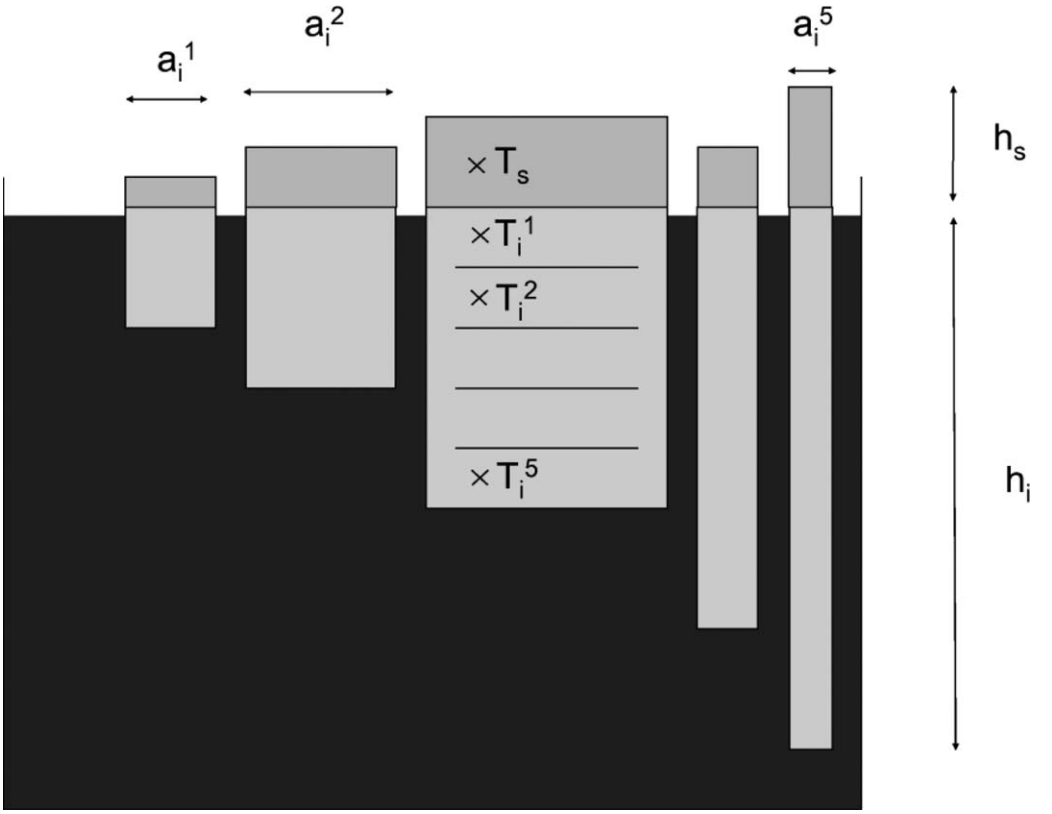

Figure 2. Scheme of the representation of sea ice in the LIM3 model, showing the L = 5 thickness categories, horizontally uniform with unique ice thickness (hil) and snow depth (hsl) and characterized by a relative coverage a^l. In each ice thickness category, the snow-ice column is vertically divided into one layer of snow and N = 5 layers of sea ice.

The temperature at the snow-ice interface (Figure 1b) is used to compute the air-ice CO_2 flux in each sea ice thickness category, using the empirical relationship of Figure 1b:

$$F^l_{CO_2} = F_{CO_2}(T^l_{si}). \quad (2)$$

Finally, the net, air-ice CO_2 flux over all ice categories in the model grid cell is given by

$$F^{air-ice}_{CO_2} = \sum_{l=1}^{5} a^l_i F^l_{CO_2}. \quad (3)$$

Note that, as flooding affects the CO_2 dynamics, points with surface flooding were excluded in the present analysis. Snow-ice formation occurs in the model if the snow load is large enough to depress the snow-ice interface under the sea level. The flooded snow is transformed into ice by applying heat and mass conservation.

Following the setup detailed in *Vancoppenolle et al*. [2008], we conducted a hindcast simulation of the Antarctic sea ice pack over 1976–2007, using a combination of daily NCEP reanalyses of air temperature and winds [*Kalnay et al*., 1996] and of various climatologies to compute the thermodynamic and dynamic forcings of the model. In addition, the simulation includes the diagnostic air-ice CO_2 flux. The time step is 1.6 h for the ocean and 8 h for the sea ice.

3. Results and Discussion

3.1. Changes in pCO_2 of Brines and Air-Ice CO_2 Fluxes During Sea Ice Warming

3.1.1. pCO_2 of Brines

Sea ice-brine pCO_2 decreased dramatically as sea ice warmed (Figure 1a) and the brines shifted from a large CO_2 oversaturation ($\Delta pCO_2 = pCO_{2(brines)} - pCO_{2(air)} = 525$ ppm) during early spring (October) to a marked undersaturation ($\Delta pCO_2 = -335$ ppm) during summer (December). The sea ice brine pCO_2 appears to be tightly related to sea ice temperature.

As the ice temperature increases, ice crystals melt and salinity decreases accordingly. We explored the relationships among brine pCO_2, temperature, and salinity by carrying out a stepwise simulation of conservative dilution of early spring-time brine collected during 2003/V1 cruise during warming at thermal brine-ice equilibrium. In details, (i) we calculated brine salinity at a given temperature according to the relationship of *Cox and Weeks* [1983]; (ii) we normalized mean TA and DIC to a salinity of 35 (TA_{35}, and DIC_{35}, respectively) for the two coldest brines collected during 2003/V1 cruise; (iii) we computed TA_t and DIC_t at a given temperature, t (and related salinity) assuming a conservative behavior of TA and DIC; and (iv) computed the brine pCO_2 for each temperature from TA_t and DIC_t, using CO_2 acidity constants of *Dickson and Millero* [1987]. Here we assume that these constants are valid for the range of temperatures and salinities encountered within the sea ice [*Delille et al*., 2007; *Papadimitriou et al*., 2004]. The resulting pCO_2-temperature relationship is shown in Figure 1a (red dashed curve). The dilution effect largely encompasses the thermodynamic effect of temperature increase on pCO_2 and the pattern of observed pCO_2 matches the theoretical variation related to both processes. This suggests that a large part of the spring pCO_2 drawdown is driven by the dilution of brines associated with the melting of ice crystals as temperature increases. Conversely, the oversaturation observed at the end of winter can result from brine concentration during sea ice growth and cooling.

3.1.2. CO_2 Fluxes

While air-ice CO_2 fluxes were not detectable below $-8°C$ (Figure 1b), we observed positive fluxes up to $+1.9$ mmol m^{-2} d^{-1} between -8 and $-6°C$ (where a positive flux corresponds to a release of CO_2 from the ice to the atmosphere). Above $-6°C$, air-ice CO_2 fluxes decrease down to -5.2 mmol m^{-2} d^{-1} in parallel with the increase of temperature. These fluxes are of the same order of magnitude as the fluxes reported by *Nomura et al*. [2013] over land fast ice. Higher sinks (negative fluxes: -6.6 to -18.2 mmol m^{-2} d^{-1}) have been reported in Antarctica [*Zemmelink et al*., 2006]. These were carried out using eddy covariance over a slush ice—a mixture of melting snow, ice, and flooding seawater covering the sea ice. Note, however, that computations of *Zemmelink et al*. [2006] should be considered with caution, since they did not take into account at the time proper corrections required for open-path CO_2 analyzer in cold temperature [*Burba et al*., 2008].

Table 2. Estimates of Potential pCO_2 Changes Related to Spring and Summer Physical and Biogeochemical Processes Observed During the 2003/V1 and ISPOL Cruises

	Related Changes						
	Temperature (°C)	Salinity (of Brines)	TA (μmol kg^{-1} of Bulk Ice)	DIC (μmol kg^{-1} of Bulk Ice)	TA (μmol kg^{-1} of Brines)	DIC (μmol kg^{-1} of Brines)	pCO_2 (ppm in Brines)
Temperature increase and related dilution	5.9	−94	0	0	−2125	−1813	−684
Primary production	0	0	4.1	−25.8	107	−669	−639
$CaCO_3$ dissolution	0	0	157.2	78.6	4075	2038	−583

3.2. Assessment of Atmospheric CO_2 Uptake by Antarctic Sea Ice From the Relative Contribution of Processes Controlling Sea Ice pCO_2

Impurities expulsion (that might be enhanced for CO_2 compared to salt [*Loose et al*., 2009]) changes in brines concentration, precipitation, or dissolution of carbonate [*Anderson and Jones*, 1985; *Delille et al*., 2007; *Papadimitriou et al*., 2004, 2007; *Rysgaard et al*., 2007], abiotic release or uptake of gaseous CO_2, primary production, and respiration all contribute to CO_2 dynamics [*Delille et al*., 2007; *Søgaard et al*., 2013] in sea ice. In this section, we will describe those processes and provide an estimate of their relative contribution to spring and summer pCO_2 changes in sea ice. We estimated the potential maximal individual impact of thermodynamic, chemical and biological processes (temperature increase and related dilution, carbonate dissolution and primary production) to the spring-summer decrease of pCO_2 (Table 2). The variations are computed from the conditions of temperature, bulk ice salinity, TA_{35}, and pCO_2 (−7.2°, 5.4, 791 μmol kg^{-1}, 724 ppm, respectively) corresponding to the average of the two coldest conditions encountered during the 2003/V1 (coldest end term of the solid curve in Figure 1a) and ISPOL cruises. Related changes during the spring to summer transition are discussed in the sections below.

3.3. Changes in Brines Concentration

In autumn and winter, decrease of temperature leads to the concentration of solutes in brines inclusions which induce high pCO_2 within sea ice brines as observed in Figure 1a. In spring and summer, as the temperature increases, the melt of ice crystals and the subsequent dilution of the brines promote a decrease of the sea ice brine pCO_2. For all our cruises, temperature increased from −7.2°C to −1.3°C (corresponding to an increase of 5.9°C in Table 2) with a decrease of the brine salinity from 117.1 to 23.5 (corresponding to a salinity change of −94 in Table 2) according to relationships of *Cox and Weeks* [1983].

The decrease in salinity, related to the rise of temperature, leads to the dilution of DIC and TA. This induces a computed pCO_2 drop of 684 ppm (Table 2), using the CO_2 dissociation constants of *Mehrbach et al*. [1973] refitted by *Dickson and Millero* [1987]. Brine dilution by internal melting appears to account for a significant part of the observed pCO_2 spring drawdown.

3.4. Primary Production

While sympagic algae are still active in autumn and winter, their photosynthetic rate should be limited by light availability, low temperatures, high salinity, and restricted space for growth [*Arrigo et al*., 1997; *Mock*, 2002], and this contribution to the DIC normalized to a constant salinity of 35 (DIC_{35}) winter removal observed in Figure 3 is therefore likely small.

Estimating primary production in sea ice—and the related impact on pCO_2—is challenging. We assumed the overall sea ice primary production prior to and during the ISPOL cruise corresponded to the autotrophic organic carbon ($OC_{autotroph}$) standing stock in the ice at the end of the ISPOL cruise. This autotrophic organic carbon was estimated from Chl *a* measurements (at 6 depths) presented in *Lannuzel et al*. [2013] and a C:Chl *a* ratio of 83. This ratio was determined by comparing Chl *a* concentration and $OC_{autotroph}$ content derived from abundance and biovolume of autotrophic organisms measured from inverted and epifluorescence microscopy observations, and carbon:volume conversion factors [*Hillebrand et al*., 1999; *Menden-Deuer and Lessard*, 2000].

The autotrophic organic carbon amount could be underestimated because it does not take into account losses of autotrophic organic carbon (i.e., mortality, exchange with the underlying seawater). On the other

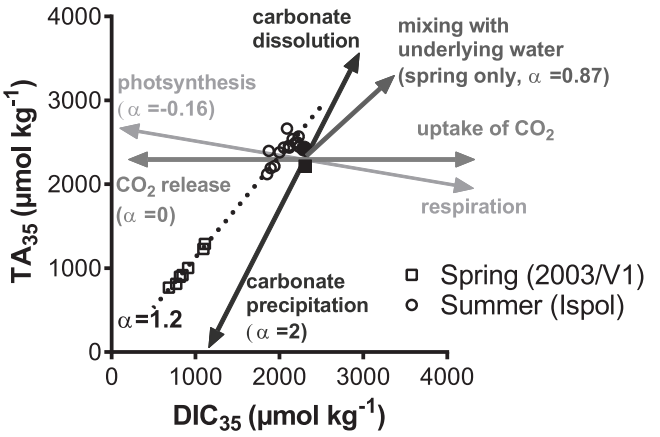

Figure 3. Normalized DIC to a constant salinity of 35 (DIC_{35}) against normalized TA (TA_{35}). Open squares and open circles denote spring (2003/V1 cruise) and summer (ISPOL cruise) samples, respectively. The slope of the corresponding regression line is reported as "α." Solid square and circle report the average of all under-ice measurements carried during 2003/V1 and ISPOL cruise, respectively (the corresponding average pCO_2 are 417 and 390 ppm, respectively). Arrows represent the theoretical variation of DIC_{35} and TA_{35} due to biogeochemical processes (i.e., photosynthesis/respiration, calcium carbonate dissolution/precipitation, mixing with underlying water, uptake/release of CO_2 with the atmosphere or bubbles trapped within the ice). The theoretical slopes of the relative variation of TA35 and DIC35 of each biogeochemical process are given (number between parentheses).

hand, we neglected the part of autotrophic community originating from organisms trapped during sea ice growth and autumnal primary production. At the end of the ISPOL cruise, the mean Chl *a* concentration was 3.7 μg kg^{-1} of bulk ice, which corresponds to an $OC_{autotroph}$ standing stock of 309 μg C kg^{-1} of bulk ice. The buildup of the $OC_{autotroph}$ standing stock would correspond to an uptake of DIC of 25.8 μmol kg^{-1} in bulk ice and an increase of TA of 4.1 μmol kg^{-1} of bulk ice, according to the Redfield-Ketchum-Richards stoichiometry of biosynthesis [*Redfield et al*., 1963; *Richards*, 1965]. With the volume of brines derived from the equations of *Cox and Weeks* [1975], revisited by *Eicken* [2003], this leads to a DIC decrease of 669 μmol kg^{-1} of brines and a TA increase of 107 μmol kg^{-1} of brines (Table 2) and a subsequent decrease of the of brines pCO_2 of 639 ppm (Table 2). The buildup of the $OC_{autotroph}$ standing stock would also correspond to a primary production of 0.26 g C m^{-2} considering an ice thickness of 90 cm (average ice thickness during the ISPOL survey).

3.5. Calcium Carbonate

Figure 3 provides insights on the processes occurring within sea ice prior and during our surveys. We plotted normalized DIC_{35} versus normalized TA (TA_{35}) in order to distinguish which processes, other than dilution/concentration and temperature changes, control the carbonate system. Normalization removes the influence of dilution/concentration, while temperature changes do not affect DIC and TA. The biogeochemical processes that can potentially affect DIC_{35} and TA_{35} are reported as solid bars. TA_{35} and DIC_{35} of brines in spring are significantly lower than in the underlying water. Differences between brines and the underlying water decrease in summer. TA_{35} and DIC_{35} in both spring and summer are remarkably well correlated with a slope of 1.2. Carbonate dissolution/precipitation best explain the observed trend, although the theoretical slope should be 2. Such a discrepancy might be due to uptake of gaseous CO_2 (from bubbles or the atmosphere) combined with carbonate dissolution, mixing with underlying water owing to internal convection, or enhanced gas expulsion [*Golden et al*., 1998; *Loose et al*., 2009; *Weeks and Ackley*, 1986]. The low TA_{35} value observed during 2003/V1 cruise suggests that carbonate precipitation occurred within sea ice prior to the cruise.

Rysgaard et al. [2007] suggested that precipitation of calcium carbonate in sea ice can act as a significant sink for atmospheric CO_2. However, there are still some crucial gaps in the current understanding of carbonate precipitation in sea ice. In particular, available field experiments hardly addressed the timing and conditions of carbonate precipitation in natural sea ice. Knowing these conditions is nevertheless crucial to assess the role played by sea ice carbonate precipitation as a sink or source of CO_2 for the atmosphere. In order to bring some attention on the need to better constrain $CaCO_3$ precipitation in natural sea ice, we consider below different scenarios of $CaCO_3$ precipitation and explore how air-ice CO_2 fluxes depend on the condition of $CaCO_3$ precipitation. Furthermore, the fate of carbonate precipitates is a good illustration of how intricate the links between biogeochemical and physical sea ice processes are (Figure 4). Based on field studies, "excess" TA in the water column during sea ice melting was attributed to the dissolution of calcium carbonate precipitated in brines and released into the underlying water [*Jones et al*., 1983; *Rysgaard et al*., 2007]. Precipitation of calcium carbonate as ikaite ($CaCO_3.6H_2O$) crystals has been observed both in the

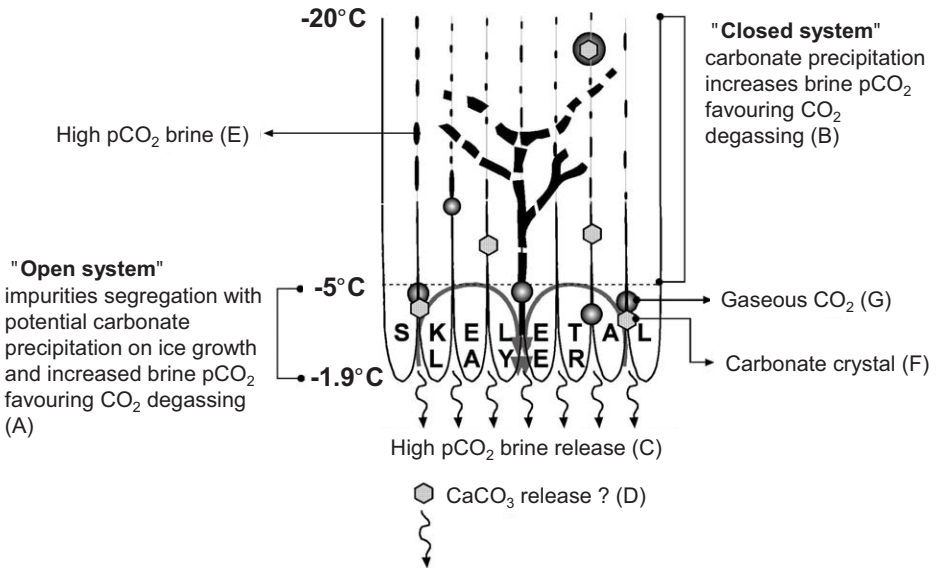

Figure 4. Fate of carbonate solids precipitated within sea ice.

Arctic and the Antarctic sea ice [*Dieckmann et al*., 2008, 2010; *Geilfus et al*., 2013; *Rysgaard et al*., 2007, 2013; *Søgaard et al*., 2013].

If carbonate precipitates in high salinity-low temperature conditions, such precipitation would likely take place in late autumn or winter in the upper layers of sea ice while brines channels are closed (Figure 4B). This precipitation produces CO_2. If brines channels are closed, this CO_2 is not transported elsewhere. For instance *Killawee et al*. [1998] and *Tison et al*. [2002] already observed CO_2-rich bubbles in artificial sea ice and suggested that they could be issued from carbonate precipitation. During spring internal melting, dissolution of carbonate solids formed in fall and winter should consumes CO_2 in the same amount as it was produced by precipitation. The net uptake of atmospheric/sea water CO_2 related to the production and dissolution of carbonate in that case would be nil over the period.

In the opposite, the phase diagram of *Assur* [1958] and the work of *Richardson* [1976] suggest that ikaite could precipitate at relatively high temperature (−2.2°C) and low salinity. Under these conditions, carbonate precipitation might potentially take place in the skeletal layer (the lamellar ice-water interface, a relatively open system) during sea ice growth (Figure 4F). At the ice-water interface, the segregation of impurities enhances CO_2 concentration at the ice-water interface during ice growth [*Killawee et al*., 1998] and acts as a source of CO_2 for the underlying layer. CO_2 produced by the precipitation can either be expelled to the underlying water layer (Figure 4C) or released to the atmosphere, especially in young thin permeable sea ice [*Geilfus et al*., 2013]. A crucial issue is the fate of carbonate solids formed in the skeletal layer. They can either (a) sink (Figure 4F) in the underlying layer faster than the CO_2 rich brines (Figure 4D). In that case, carbonate precipitation acts as a net source of CO_2 for the atmosphere, especially if some CO_2-rich brines trapped within sea ice are connected to the atmosphere in spring and summer (Figure 4E). (b) Carbonate solids may sink at the same rate than the brines that transport produced CO_2 with negligible impact on DIC budget of the water column and the impact for the atmosphere is nil. (c) Carbonate solids remain trapped in the tortuosity of the skeletal layer while CO_2 produced by the precipitation is expelled to the underlying water with the brines (Figure 4C) and entrained toward deep layers due to the high density of brines. The dissolution of trapped carbonate solids in spring and summer triggered by temperature increases and related salinity decreases, would consume CO_2 and drive CO_2 uptake within the ice. In that case, carbonate precipitation acts as a sink for atmospheric CO_2. However, *Papadimitriou et al*. [2013] showed recently that at −2.2°C carbonate precipitation can occur only in low pCO_2 conditions that are uncommon below sea ice during sea ice formation.

Taking into account the estimates of the saturation state of ikaite as a function of brine pCO_2 and temperature provided by *Papadimitriou et al*. [2013] and taking into account the pCO_2 versus temperature

Table 3. Estimates of Potential Air-Ice CO_2 Fluxes In Order To Restore Equilibrium Following Changes in Brine pCO_2 Associated to Spring and Summer Physical and Biogeochemical Processes Observed During the 2003/V1 and ISPOL Cruises[a]

Process	Related CO_2 Transfer From the Atmosphere (mmol m^{-2})
Temperature increase and related dilution	−60
$CaCO_3$ dissolution	−57
Primary production	−25
Total	−141

[a]Flux representative of a 4 month period.

relationship of Figure 1a, it seems reasonable that the threshold of saturation of ikaite for brine corresponds to temperature ranging between −5°C and −6°C. So when the ice cools down, carbonate precipitation can potentially develop below −5°C. If the bulk salinity of ice is above 5, then at −5°C, the brine volume is above 5% [*Cox and Weeks*, 1983; *Eicken*, 2003] and ice is permeable [*Golden et al*., 1998]. In these conditions, fluids still percolate and transport CO_2 while solid particles remain trapped due to the tortuosity of the ice matrix. This corresponds to the previous (c) scenario.

This leads to the segregation between carbonate precipitates, which remain trapped within sea ice while the CO_2 produced is expelled to the underlying water with brines. Such a mechanism could act as an efficient pump of CO_2 from the atmosphere. The expulsion of brines enriched in CO_2 leads to the formation of dense water that sinks rapidly during sea ice growth. The sinking of dense water is the main driver of deep-water formation and is potentially an efficient CO_2 sequestration pathway. Numerous vertical distributions profiles of TA below sea ice have revealed the signature of carbonate precipitation [*Weiss et al*., 1979]. When sea ice melts during spring and summer, trapped carbonate solids dissolve as the result of the combined increase of temperature and decrease of salinity either within sea ice or in the underlying water. This dissolution of carbonate solids observed by *Jones et al*. [1983] leads to a decrease of pCO_2 and might act as an efficient and significant sink of CO_2 according to observations and models [*Rysgaard et al*., 2007, 2011, 2012; *Søgaard et al*., 2013]. However, as underlined before, part of that process might not be a net annual sink if carbonate precipitate in permeable sea ice, and that the produced CO_2 degasses to the atmosphere [*Geilfus et al*., 2013].

Low values of DIC_{35} and TA_{35} in brines collected in early spring in cold sea ice (Figure 3) indicate that carbonate precipitation occurred within brines prior to the 2003/V1 cruise, further eastward. The imprint of carbonate precipitation is well marked, leading to a decrease of 65% of TA_{35} in brines, compared to the underlying water (Figure 3). Such difference would correspond to the precipitation of carbonate of about 2038 μmol kg^{-1} from the brines, assuming the effect of fall and winter microbial activity on TA is negligible. Carbonate precipitation will reduce the DIC_{35} and increase pCO_2 as the brine salinity increases during ice growth. This will contribute to the winter oversaturation of CO_2. If we assume that the carbonate solids remain trapped within the ice and no CO_2 is stored in the gaseous phase within sea ice during the cooling processes, then spring dissolution would reduce pCO_2 by about 583 ppm (Table 3).

However, the observed decrease in TA_{35} due to carbonate precipitation corresponds theoretically to a removal of 30% of DIC_{35}, while the overall decrease of DIC_{35} reaches 70% at the coldest temperature (Figure 3). Thus, about 40% of DIC_{35} reduction has to be ascribed to either autumnal/winter primary production or CO_2 transfer to the gas phase within the brines or enhanced gas expulsion compared to salt [*Loose et al*., 2009]. For instance, *Geilfus et al*. [2013] report significant release of CO_2 from the ice to the atmosphere as a result of solutes expulsion during early stages of ice formation.

3.6. First-Order Assessment of Air-Ice CO_2 Transfers Over Antarctic Sea Ice

The potential air-ice CO_2 transfers related to sea ice physical and biogeochemical processes were assessed by considering a homogeneous 90 cm thick sea ice cover in equilibrium with the atmosphere and isolated from exchange with the underlying water. The sea ice thickness value is the mean observed during the ISPOL experiment and is low compared to the values generally observed in the Weddell Sea and elsewhere [*Haas et al*., 2003; *Timmermann et al*., 2002]. Temperature, salinity, and $\delta^{18}O$ data [*Tison et al*., 2008] suggest that low exchanges occurred between sea ice and the underlying layer during the ISPOL experiment. We assumed that sea ice was initially in equilibrium with the atmosphere (pCO_2 = 370 ppm), and we applied the biogeochemically driven DIC and TA changes of Table 3 (expressed per kilogram of bulk ice), and then computed the air-ice CO_2 transfers required to restore equilibrium. We used the brine volume values computed from the equations of *Cox and Weeks* [1975] revisited by *Eicken* [2003] and mean conditions observed

during the two last ISPOL stations (mean sea ice temperature: −1.3°C, mean brine salinity: 24, mean bulk ice salinity: 3.8, and mean TA: 1667 μmol kg^{-1} of brines). For the uptake owing to temperature change and related dilution effect, we considered a temperature increase from −7.2 to −1.3°C corresponding to the range of observations during the 2003/V1 and ISPOL cruises, salinity decrease from 117 to 24, and decrease of TA from 8135 to 1667 μmol kg^{-1} of brines so that TA_{35} remains constant.

For an Antarctic first year sea ice surface area of 14×10^6 km^2 [*Comiso*, 2003], the corresponding upscaled overall CO_2 uptake due to those cumulated three processes (Table 3) is 0.024 Pg C for spring-summer.

3.7. Comparison of the Significance of the Main Processes on CO_2 Uptake

Tables 2 and 3 provide some insights on the relative contribution of the three main processes (increase of temperature and related dilution, primary production, and dissolution of carbonate solids) to the pCO_2 drawdown and the uptake of atmospheric CO_2. It must keep in mind that the assessment of the contribution of primary production is less robust than the other assessments. As observed by *Delille et al*. [2007] in Antarctic land fast ice, the impact on pCO_2 of warming and related dilution is similar to those of dissolution of carbonate solids. The contribution of primary production is only slightly lower (Table 2). In terms of CO_2 uptake, the contribution of primary production represents only 45% of the contribution of each other process, but it still significant. In contrast *Søgaard et al*. [2013] in subarctic land fast suggest that the contribution of primary production to the uptake of atmospheric CO_2 is pretty small compared to the other processes. However, these differences should reflect the differences in primary production between different areas.

3.8. Assessment of Atmospheric CO_2 Uptake by Antarctic Sea Ice From Fluxes: Sea Ice Temperature Relationship in a 3-D Model

We measured CO_2 fluxes over widespread sea ice without biologically active surface communities. Previous eddy correlation CO_2 fluxes measurements were carried out over areas covered by particular surface environments, namely melt ponds and slush [*Semiletov et al*., 2004; *Zemmelink et al*., 2006]. Slush is known to hosts a highly productive algae community [*Legendre et al*., 1992]. Sea ice surface communities benefit from high light levels and from nutrients from seawater flooding as snow loading or sea ice rafting depresses the ice surface below the freeboard. Such surface flooding occurs over 15–30% of the ice pack in Antarctica [*Wadhams et al*., 1987]. These surface communities exhibit photosynthetic rates comparable to those of open ocean Antarctic phytoplankton [*Lizotte and Sullivan*, 1992] and might be responsible for the majority of sea surface productivity in Antarctic sea ice [*Legendre et al*., 1992]. They easily exchange CO_2 with the atmosphere through the porous snow cover and can potentially enhance significantly the estimate for CO_2 uptake by the sea ice cover given below.

In a heterogeneous environment like sea ice, the small spatial resolution of the chamber CO_2 flux measurements allows a consistent comparison with pCO_2 within the ice. The pCO_2 gradient between the atmosphere and the brines in the sea ice top layer is the main driver of CO_2 fluxes. The CO_2 fluxes are consistent with the saturation level of CO_2 in the brines. No CO_2 flux was detected below −10°C suggesting that sea ice was then virtually impermeable to CO_2 exchange (Figure 1b). At a temperature of ∼−7°C, the low permeability of the ice results in weak net CO_2 fluxes despite elevated pCO_2. As the temperature increases, pCO_2 of the ice decreases and sea ice shifts from a transient CO_2 source to a sink.

The fluxes are modulated by factors like sea ice temperature and snow and ice structure [*Geilfus et al*., 2012; *Nomura et al*., 2010, 2013]. While snow allows exchange of gases with the atmosphere [*Albert et al*., 2002; *Massman et al*., 1997; *Takagi et al*., 2005], very low to nil fluxes were observed after the formation of lenses of superimposed ice above sea ice (diamonds in Figure 1b) that was detected at the sampling site and elsewhere during ISPOL cruise [*Nicolaus et al*., 2009]. Superimposed ice forms after a strong snow melt event when percolating freshwater refreezes at the contact of proper sea ice [*Haas et al*., 2001]. As freshwater ice, the superimposed ice is impermeable to gas transport [*Albert and Perron*, 2000]. The formation of superimposed ice at the top of sea ice observed at certain stations during ISPOL cruise is the best candidate to explain the inhibition of air-ice CO_2 fluxes at those stations. During superimposed ice events, ongoing strong dilution of the brine by the melting sea ice was decreasing brine pCO_2. Development of superimposed ice impeded CO_2 transfer from the atmosphere to the sea ice that normally should drive pCO_2 values toward the atmospheric concentration. As a result, drastic decreases of brine pCO_2 down to 30 ppm were observed during superimposed ice events. This highlights the role of CO_2 invasion from the atmosphere

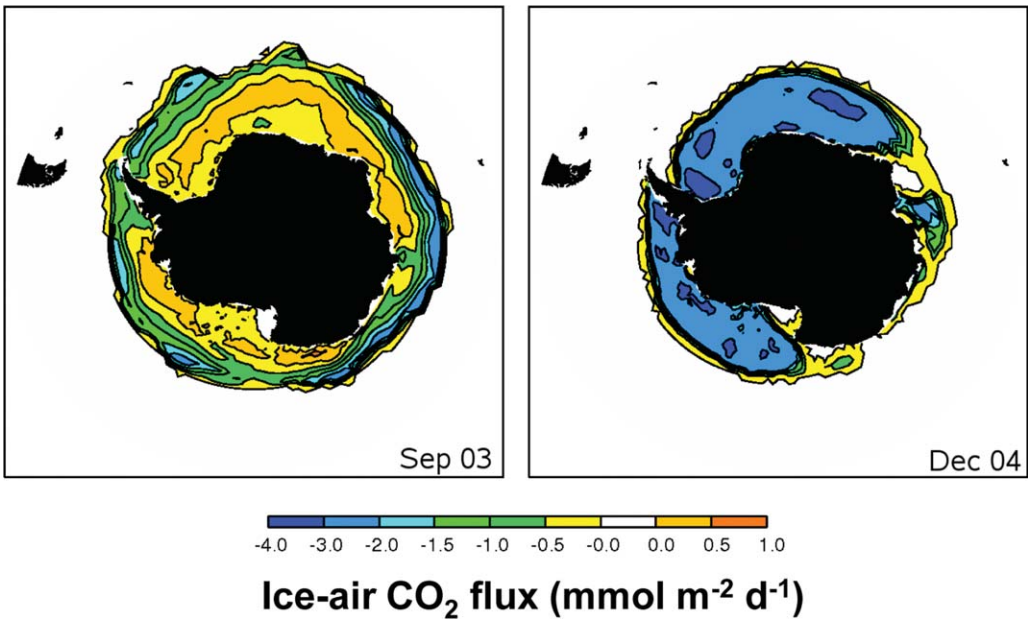

Figure 5. Distribution of the ice-air CO_2 flux (mmol C m^{-2} d^{-1}) over the Antarctic sea ice zone, in September 2003 (a, corresponding to the period of the 2003/V1 cruise) and in December 2004 (b, corresponding to the period of the ISPOL cruise), reconstructed from ice temperature simulated by NEMO-LIM3 model, for ice concentrations >65%.

that balances the summer pCO_2 drawdown sustained by dilution and primary production and maintains sea ice pCO_2 above 100 ppm.

Despite the effect of snow and ice structure on fluxes, sea ice temperature appears to exert a crucial control on both sea ice pCO_2 gradient, gas transfer through permeability, and ultimately on CO_2 transfer at the air-ice interface (Figure 1b). We therefore derived an empirical relationship between CO_2 flux and sea ice temperature (Figure 1b) allowing the reconstruction of CO_2 flux fields (Figure 5) using sea ice temperature, concentration, and coverage from the NEMO-LIM3 large-scale sea ice-ocean model [*Madec*, 2008; *Vancoppenolle et al*., 2008]. Spring and summer air-ice CO_2 fluxes were estimated from 1997 to 2007 for nonflooded areas with ice concentration above 65% (Figure 6), corresponding to the range of sea ice concentration encountered during sampling. This upscaling suggests that Antarctic sea ice cover pumps 0.029 Pg C of atmospheric CO_2 (Table 4) into the ocean during the spring-summer transition.

This assessment corroborates the first-order independent assessment derived from pCO_2 dynamics relative to each main process (see previous section). Both CO_2 sink estimates most probably underestimate the uptake of CO_2 over Antarctic sea ice as they do not account for (1) areas with sea ice concentration <65%, (2) flooded areas, and (3) surface communities that may significantly enhance CO_2 uptake.

4. Conclusion

The elevated sea ice pCO_2 in winter results from an intricate superimposition of counteracting processes: those increasing pCO_2 such as brine concentration and carbonate precipitation, and those decreasing pCO_2 such as enhanced gas expulsion, autumnal primary production, temperature decrease, and CO_2 transfer to the gaseous phase.

In spring, we observed a sharp decrease of pCO_2 that is tightly related to sea ice melting and related brine dilution. We also show that carbonate dissolution could induce pCO_2 changes comparable to those attributed to dilution. In summer, as sea ice becomes isothermal, dilution effects level off. At that stage, uptake of atmospheric CO_2 and mixing with underlying water (with pCO_2 values ranging from 380 to 430 ppm) should maintain pCO_2 at or above the saturation level. However, sustained primary production appears to be large enough to maintain low pCO_2 within the sea ice. One should note that we did not address CO_2 uptake from the underlying to the ice driven by bottom sympagic communities and CO_2 transfer from the

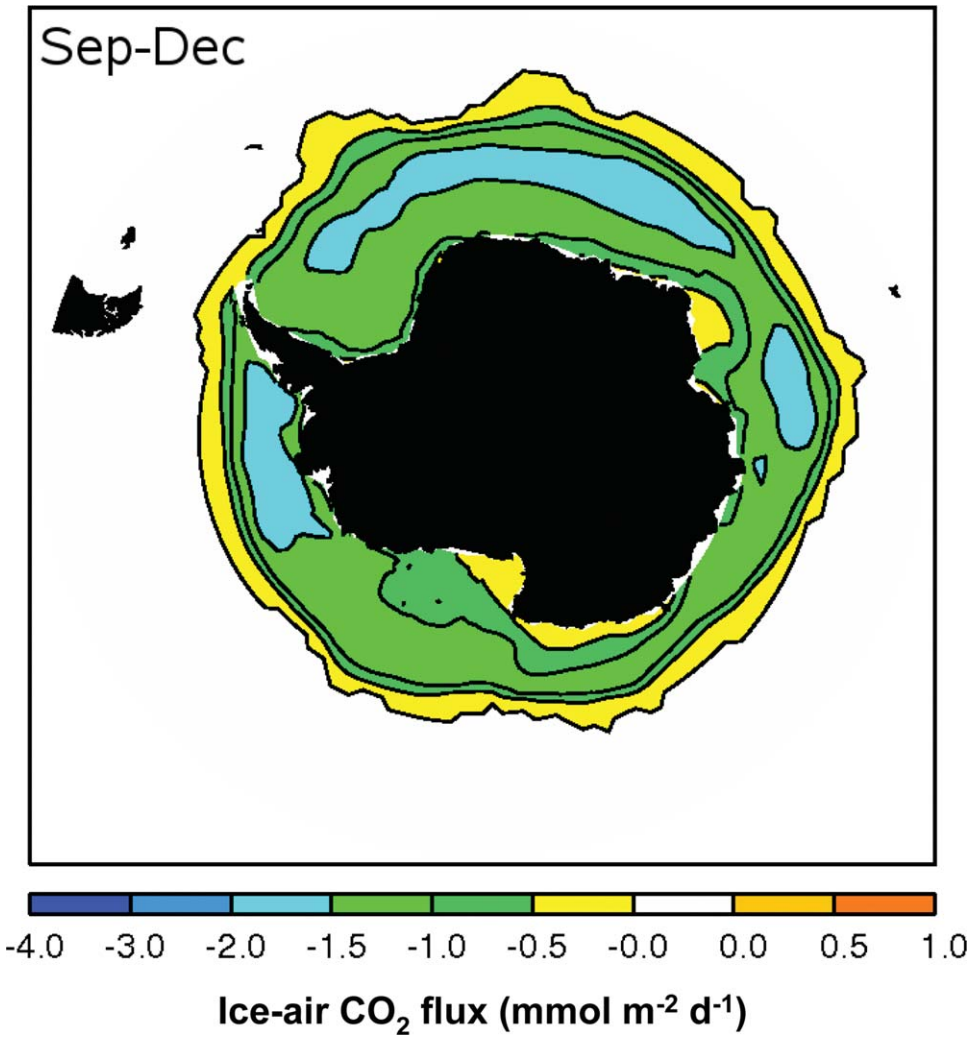

Figure 6. Average September to December distribution of the ice-air CO_2 flux over the Antarctic sea ice zone (mmol C m^{-2} d^{-1}) as simulated by the sea ice model, during the 1997–2007.

underlying water to the atmosphere through the ice that are considered insignificant [*Loose et al.*, 2011; *Rutgers van der Loeff et al.*, 2014].

Table 4. Spring and Summer Air-Ice CO_2 Fluxes Assessed With the NEMO-LIM3 Model From 1997 to 2009

Year	Total CO_2 Sink (Pg C)
1997	−0.0273
1998	−0.0272
1999	−0.0289
2000	−0.0301
2001	−0.0274
2002	−0.0301
2003	−0.0299
2004	−0.0293
2005	−0.0298
2006	−0.0287
2007	−0.0291
Mean	−0.0289
STD	0.0011

These processes act as sink for atmospheric CO_2. Using the relative contribution of the main processes driving pCO_2 in sea ice, we derived an uptake of 0.024 Pg C for spring and summer. This assessment corroborates the estimate from in situ CO_2 flux measurements scaled with the ice temperature simulated with the NEMO-LIM3 model that is assessed to 0.029 Pg C. Both assessments compare favorably with the assessments of *Rysgaard et al.* [2011] of 0.019 and 0.052 Pg C yr^{-1} for the CO_2 fluxes over the whole Southern Ocean, respectively "without" and "with" $CaCO_3$ formation in sea ice.

We consider that the fluxes derived from the NEMO-LIM3 are the best estimate to date of the uptake of atmospheric CO_2 by Antarctic sea ice in spring and

summer. Accordingly, sea ice provides an additional significant sink of atmospheric CO_2 in the Southern Ocean up to 58% of the estimated net uptake of the Southern Ocean south of 50°S (0.05 Pg C yr^{-1}) [*Takahashi et al.*, 2009]. Antarctic pack ice appears to be a significant contributor of CO_2 fluxes in the Southern Ocean. We believe that our approach is conservative since we excluded areas with ice concentration below 65% and flooded zones.

Acknowledgments

The authors appreciated the kindness and efficiency of the crews of *R.S.V. Aurora Australis*, *R.V. Polarstern*, and *R.V. N.B. Palmer*. We are grateful to Tom Trull, Steve Ackley, and two anonymous reviewers for their useful comments that improved the quality of the manuscript. This research was supported by the Belgian Science Policy (BELCANTO projects, contract SD/CA/03A), the Belgian French Community (SIBCLIM project), the F.R.S.-FNRS and the Australian Climate Change Science Program. NXG received a PhD grant from the Fonds pour la Formation à la Recherche dans l'Industrie et l'Agriculture and now received financial support from the Canada Excellence Research Chair (CERC) program. BD is a research associate of the F.R.S.-FNRS. VS benefits from a COFUND Marie Curie fellowship "Back to Belgium Grant." Supplemental data used to produce figures are freely available at the address www.co2.ulg.ac.be/data/Delille_et_al_supplemental_data.xlsx. This is MARE contribution 276.

References

Albert, M. R., and F. E. Perron (2000), Ice layer and surface crust permeability in a seasonal snow pack, *Hydrol. Processes*, *14*(18), 3207–3214.

Albert, M. R., A. M. Grannas, J. Bottenheim, P. B. Shepson, and F. E. Perron (2002), Processes and properties of snow-air transfer in the high Arctic with application to interstitial ozone at Alert, Canada, *Atmos. Environ.*, *36*(15–16), 2779–2787.

Anderson, L. G., and E. P. Jones (1985), Measurements of total alkalinity, calcium and sulfate in natural sea ice, *J. Geophys. Res.*, *90*(C5), 9194–9198, doi:10.1029/JC090iC05p09194.

Arrigo, K. R. (2003), Primary production in sea ice, in *Sea Ice: An Introduction to Its Physics, Chemistry, Biology and Geology*, edited by D. N. Thomas and G. Dieckmann, pp. 143–183, Blackwell Sci., Oxford, U. K.

Arrigo, K. R., D. L. Worthen, M. P. Lizotte, P. Dixon, and G. Dieckmann (1997), Primary production in Antarctic sea ice, *Science*, *276*, 394–397, doi:10.1126/science.276.5311.394.

Assur, A. (1958), Composition of sea ice and its tensile strength, in *Arctic Sea Ice*, pp. 106–138, Natl. Acad. of Sci.-Natl. Res. Counc., Washington, D. C.

Buckley, R. G., and H. J. Trodahl (1987), Thermally driven changes in the optical properties of sea ice, *Cold Reg. Sci. Technol.*, *14*(2), 201–204.

Burba, G., D. K. McDermitt, A. Grelle, D. J. Anderson, and L. Xu (2008), Addressing the influence of instrument surface heat exchange on the measurements of CO_2 flux from open-path gas analyzers, *Global Change Biol.*, *14*(8), 1854–1876, doi:10.1111/j.1365-2486.2008.01606.x.

Comiso, J. C. (2003), Large-scale characteristics and variability of the global sea ice cover, in *Sea Ice: An Introduction to Its Physics, Chemistry, Biology and Geology*, edited by D. N. Thomas and G. Dieckmann, pp. 112–142, Blackwell Sci., Oxford, U. K.

Copin-Montégut, C. (1988), A new formula for the effect of temperature on the partial pressure of carbon dioxide in seawater, *Mar. Chem.*, *25*(1), 29–37.

Cox, G. F. N., and W. F. Weeks (1975), Brine drainage and initial salt entrapment in sodium chloride ice. CRREL Research Rept 345, 85 pp.

Cox, G. F. N. and W. F. Weeks (1983), Equations for determining the gas and brine volumes in sea-ice samples, *J. Glaciol.*, *29*(102), 306–316.

Delille, B., B. Jourdain, A. V. Borges, J. L. Tison, and D. Delille (2007), Biogas (CO_2, O_2, dimethylsulfide) dynamics in spring Antarctic fast ice, *Limnol. Oceanogr.*, *52*(4), 1367–1379, doi:10.4319/lo.2007.52.4.1367.

Dickson, A. G., and F. J. Millero (1987), A comparison of the equilibrium constants for the dissociation of carbonic acid in seawater media, *Deep Sea Res., Part A*, *34*, 1733–1743, doi:10.1016/0198-0149(87)90021-5.

Dieckmann, G. S., G. Nehrke, S. Papadimitriou, J. Göttlicher, R. Steininger, H. Kennedy, D. Wolf-Gladrow, and D. N. Thomas (2008), Calcium carbonate as ikaite crystals in Antarctic sea ice, *Geophys. Res. Lett.*, *35*, L08501, doi:10.1029/2008GL033540.

Dieckmann, G. S., G. Nehrke, C. Uhlig, J. Göttlicher, S. Gerland, M. A. Granskog, and D. N. Thomas (2010), Ikaite ($CaCO_3$*$6H_2O$) discovered in Arctic sea ice, *Cryosphere*, *4*(2), 227–230, doi:10.5194/tc-4-227-2010.

Eicken, H. (2003), From the microscopic, to the macroscopic, to the regional scale: Growth, microstructure and properties of sea ice, in *Sea Ice: An Introduction to Its Physics, Chemistry, Biology and Geology*, edited by D. N. Thomas and G. Dieckmann, pp. 22–81, Blackwell Sci., Oxford, U. K.

Frankignoulle, M. (1988), Field measurements of air-sea CO_2 exchange, *Limnol. Oceanogr.*, *33*, 313–322.

Geilfus, N. X., G. Carnat, T. Papakyriakou, J. L. Tison, B. Else, H. Thomas, E. Shadwick, and B. Delille (2012), Dynamics of pCO_2 and related air-ice CO_2 fluxes in the Arctic coastal zone (Amundsen Gulf, Beaufort Sea), *J. Geophys. Res.*, *117*, C00G10, doi:10.1029/2011JC007118.

Geilfus, N. X., G. Carnat, G. S. Dieckmann, N. Halden, G. Nehrke, T. Papakyriakou, J. L. Tison, and B. Delille (2013), First estimates of the contribution of $CaCO_3$ precipitation to the release of CO_2 to the atmosphere during young sea ice growth, *J. Geophys. Res. Oceans*, *118*, 244–255, doi:10.1029/2012JC007980.

Gleitz, M., M. R. van der Loeff, D. N. Thomas, G. S. Dieckmann, and F. J. Millero (1995), Comparison of summer and winter in organic carbon, oxygen and nutrient concentrations in Antarctic sea ice brine, *Mar. Chem.*, *51*(2), 81–91, doi:10.1016/0304-4203(95)00053-T.

Golden, K. M., S. F. Ackley, and V. I. Lytle (1998), The percolation phase transition in sea ice, *Science*, *282*(5397), 2238–2241, doi:10.1126/science.282.5397.2238.

Gosink, T. A., J. G. Pearson, and J. J. Kelley (1976), Gas movement through sea ice, *Nature*, *263*(2), 41–42, doi:10.1038/263041a0.

Gran, G. (1952), Determination of the equivalence point in potentiometric titration, part II, *Analyst*, *77*, 661–671.

Haas, C., D. N. Thomas, and J. Bareiss (2001), Surface properties and processes of perennial Antarctic sea ice in summer, *J. Glaciol.*, *47*(159), 613–625.

Haas, C., D. N. Thomas, and G. Dieckmann (2003), Dynamics versus thermodynamics: The sea ice thickness distribution, in *Sea Ice: An Introduction to Its Physics, Chemistry, Biology and Geology*, edited by D. N. Thomas and G. Dieckmann, pp. 82–111, Blackwell Sci., Oxford, U. K.

Hillebrand, H., C. D. Durselen, D. Kirschtel, U. Pollingher, and T. Zohary (1999), Biovolume calculation for pelagic and benthic microalgae, *J. Phycol.*, *35*(2), 403–424, doi:10.1046/j.1529-8817.1999.3520403.x.

Hunke, E. C., and J. K. Dukowicz (1997), An elastic-viscous-plastic model for sea ice dynamics, *J. Phys. Oceanogr.*, *27*(9), 1849–1867, doi:10.1175/1520-0485(1997)027<1849:AEVPMF>2.0.CO;2.

Johnson, K. M., et al. (1998), Coulometric total carbon dioxide analysis for marine studies: Assessment of the quality of total inorganic carbon measurements made during the US Indian Ocean CO_2 Survey 1994–1996, *Mar. Chem.*, *63*(1–2), 21–37.

Jones, E. P., A. R. Coote, and E. M. Levy (1983), Effect of sea ice meltwater on the alkalinity of seawater, *J. Mar. Res.*, *41*, 43–52.

Kalnay, E., et al. (1996), The NCEP/NCAR 40-year reanalysis project, *Bull. Am. Meteorol. Soc.*, *77*(3), 437–471, doi:10.1175/1520-0477(1996)077<0437:TNYRP>2.0.CO;2.

Killawee, J. A., I. J. Fairchild, J. L. Tison, L. Janssens, and R. Lorrain (1998), Segregation of solutes and gases in experimental freezing of dilute solutions: Implications for natural glacial systems, *Geochim. Cosmochim. Acta*, *62*(23–24), 3637–3655, doi:10.1016/S0016-7037(98)00268-3.

Lannuzel, D., V. Schoemann, I. Dumont, M. Content, J. de Jong, J.-L. Tison, B. Delille, and S. Becquevort (2013), Effect of melting Antarctic sea ice on the fate of microbial communities studied in microcosms, *Polar Biol.*, *1–15*, doi:10.1007/s00300-013-1368-7.

Legendre, L., S. F. Ackley, G. S. Dieckmann, B. Gulliksen, R. Horner, T. Hoshiai, I. A. Melnikov, W. S. Reeburgh, M. Spindler, and C. W. Sullivan (1992), Ecology of sea ice biota 2. Global significance, *Polar Biol.*, *12*(3–4), 429–444.

Lewis, M. J. (2010), *Antarctic Snow and Sea Ice Processes: Effects on Passive Microwave Emissions and AMSR-E Sea Ice Products*, 224 pp., Univ. of Tex. at San Antonio, Tex.

Lewis, M. J., J. L. Tison, B. Weissling, B. Delille, S. F. Ackley, F. Brabant, and H. Xie (2011), Sea ice and snow cover characteristics during the winter–spring transition in the Bellingshausen Sea: An overview of SIMBA 2007, *Deep Sea Res., Part II*, *58*(9–10), 1019–1038, doi:10.1016/j.dsr2.2010.10.027.

Lizotte, M. P. (2001), The contributions of sea ice algae to Antarctic marine primary production, *Am. Zool.*, *41*(1), 57–73, doi:10.1093/icb/41.1.57.

Lizotte, M. P., and C. W. Sullivan (1992), Biochemical-composition and photosynthate distribution in sea ice microalgae of McMurdo-Sound, Antarctica—Evidence for nutrient stress during the spring bloom, *Antarct. Sci.*, *4*(1), 23–30.

Loose, B., W. R. McGillis, P. Schlosser, D. Perovich, and T. Takahashi (2009), Effects of freezing, growth, and ice cover on gas transport processes in laboratory seawater experiments, *Geophys. Res. Lett.*, *36*, L05603, doi:10.1029/2008gl036318.

Loose, B., P. Schlosser, D. Perovich, D. B. Ringelberg, D. T. Ho, T. Takahashi, Richter-Menge, J., C. M. Reynolds, W. McGillis, and J. L. Tison (2011), Gas diffusion through columnar laboratory sea ice: Implications for mixed-layer ventilation of CO_2 in the seasonal ice zone, *Tellus, Ser. B*, *63*, 23–39, doi:10.1111/j.1600-0889.2010.00506.x.

Madec, G. (2008), NEMO ocean engine, *Note du Pole de modélisation 27*, Inst. Pierre-Simon Laplace, Paris, France.

Massman, W. J., R. A. Sommerfeld, A. R. Mosier, K. F. Zeller, T. J. Hehn, and S. G. Rochelle (1997), A model investigation of turbulence-driven pressure-pumping effects on the rate of diffusion of CO_2, N_2O, and CH_4 through layered snowpacks, *J. Geophys. Res.*, *102*(D15), 18,851–18,863, doi:10.1029/97JD00844.

Massom, R. A., et al. (2006), ARISE (Antarctic Remote Ice Sensing Experiment) in the East 2003: Validation of satellite-derived sea-ice data products, *Ann. Glaciol.*, *44*, 288–296.

Mehrbach, C., C. H. Culberson, J. E. Hawley, and R. M. Pytkowicz (1973), Measurements of the apparent dissociation constants of carbonic acid in seawater at atmospheric pressure, *Limnol. Oceanogr.*, *18*, 897–907.

Menden-Deuer, S., and E. J. Lessard (2000), Carbon to volume relationships for dinoflagellates, diatoms, and other protist plankton, *Limnol. Oceanogr.*, *45*(3), 569–579, doi:10.4319/lo.2000.45.3.0569.

Miller, L. A., T. N. Papakyriakou, R. E. Collins, J. W. Deming, J. K. Ehn, R. W. Macdonald, A. Mucci, O. Owens, M. Raudsepp, and N. Sutherland (2011), Carbon dynamics in sea ice: A winter flux time series, *J. Geophys. Res.*, *116*, C02028, doi:10.1029/2009jc006058.

Mock, T. (2002), In situ primary production in young Antarctic sea ice, *Hydrobiologia*, *470*(1–3), 127–132.

Nicolaus, M., C. Haas, and S. Willmes (2009), Evolution of first-year and second-year snow properties on sea ice in the Weddell Sea during spring-summer transition, *J. Geophys. Res.*, *114*, D17109, doi:10.1029/2008JD011227.

Nomura, D., H. Eicken, R. Gradinger, and K. Shirasawa (2010), Rapid physically driven inversion of the air-sea ice CO_2 flux in the seasonal landfast ice off Barrow, Alaska after onset of surface melt, *Cont. Shelf Res.*, *30*(1), 1998–2004, doi:10.1016/j.csr.2010.09.014.

Nomura, D., M. Granskog, P. Assmy, D. Simizu, and G. Hashida (2013), Arctic and Antarctic sea ice acts as a sink for atmospheric CO_2 during periods of snow melt and surface flooding, *J. Geophys. Res. Oceans*, *118*, 6511–6524, doi:10.1002/2013JC009048.

Notz, D., and M. G. Worster (2009), Desalination processes of sea ice revisited, *J. Geophys. Res.*, *114*, C05006, doi:10.1029/2008JC004885.

Papadimitriou, S., H. Kennedy, G. Kattner, G. S. Dieckmann, and D. N. Thomas (2004), Experimental evidence for carbonate precipitation and CO_2 degassing during sea ice formation, *Geochim. Cosmochim. Acta*, *68*(8), 1749–1761, doi:10.1016/j.gca.2003.07.004.

Papadimitriou, S., D. N. Thomas, H. Kennedy, C. Haas, H. Kuosa, A. Krell, and G. S. Dieckmann (2007), Biogeochemical composition of natural sea ice brines from the Weddell Sea during early austral summer, *Limnol. Oceanogr.*, *52*(5), 1809–1823, doi:10.4319/lo.2007.52.5.1809.

Papadimitriou, S., H. Kennedy, P. Kennedy, and D. N. Thomas (2013), Ikaite solubility in seawater-derived brines at 1 atm and sub-zero temperatures to 265K, *Geochim. Cosmochim. Acta*, *109*(0), 241–253, doi:10.1016/j.gca.2013.01.044.

Papakyriakou, T. N., and L. A. Miller (2011), Springtime CO_2 exchange over seasonal sea ice in the Canadian Arctic Archipelago, *Ann. Glaciol.*, *52*, 215–224.

Poisson, A., and C. T. A. Chen (1987), Why is there little anthropogenic CO_2 in the Antarctic bottom water?, *Deep Sea Res., Part A*, *34*(7), 1255–1275.

Redfield, A. C., B. H. Ketchum, F. A. Richards, and M. N. Hill (1963), The influence of organisms on the composition of sea-water, in *The Composition of Sea-Water and Comparative and Descriptive Oceanography*, edited by M. N. Hill, pp. 26–87, Wiley-Interscience, N. Y.

Richards, F. A. (1965), *Anoxic Basins and Fjords*, edited by J. P. Riley and G. Skirrow, pp. 611–645, Academic, N. Y.

Richardson, C. (1976), Phase relationships in sea ice as a function of temperature, *J. Glaciol.*, *17*, 507–519.

Rutgers van der Loeff, M. M., N. Cassar, M. Nicolaus, B. Rabe, and I. Stimac (2014), The influence of sea ice cover on air-sea gas exchange estimated with radon-222 profiles, *J. Geophys. Res. Oceans*, *119*, 2735–2751, doi:10.1002/2013JC009321.

Rysgaard, S., R. N. Glud, M. K. Sejr, J. Bendtsen, and P. B. Christensen (2007), Inorganic carbon transport during sea ice growth and decay: A carbon pump in polar seas, *J. Geophys. Res.*, *112*, C03016, doi:10.1029/2006jc003572.

Rysgaard, S., J. Bendtsen, B. Delille, G. S. Dieckmann, R. Glud, H. Kennedy, J. Mortensen, S. Papadimitriou, D. N. Thomas, and J. L. Tison (2011), Sea ice contribution to the air–sea CO_2 exchange in the Arctic and Southern Oceans, *Tellus, Ser. B*, *63*, 823–830, doi:10.1111/j.1600-0889.2011.00571.x.

Rysgaard, S., R. N. Glud, K. Lennert, M. Cooper, N. Halden, R. J. G. Leakey, F. C. Hawthorne, and D. Barber (2012), Ikaite crystals in melting sea ice—Implications for pCO_2 and pH levels in Arctic surface waters, *Cryosphere*, *6*(4), 901–908, doi:10.5194/tc-6-901-2012.

Rysgaard, S., et al. (2013), Ikaite crystal distribution in winter sea ice and implications for CO_2 system dynamics, *Cryosphere*, *7*(2), 707–718, doi:10.5194/tc-7-707-2013.

Semiletov, I., A. Makshtas, S. I. Akasofu, and E. L. Andreas (2004), Atmospheric CO_2 balance: The role of Arctic sea ice, *Geophys. Res. Lett.*, *31*, L05121, doi:10.1029/2003GL017996.

Semiletov, I., I. Pipko, I. Repina, and N. Shakhova (2007), Carbonate chemistry dynamics and carbon dioxide fluxes across the atmosphere-ice-water interfaces in the Arctic Ocean: Pacific sector of the Arctic, *J. Mar. Syst.*, *66*(1–4), 204–226, doi:10.1016/j.jmarsys.2006.05.012.

Søgaard, D., D. Thomas, S. Rysgaard, R. Glud, L. Norman, H. Kaartokallio, T. Juul-Pedersen, and N.-X. Geilfus (2013), The relative contributions of biological and abiotic processes to carbon dynamics in subarctic sea ice, *Polar Biol.*, *36*(12), 1761–1777, doi:10.1007/s00300-013-1396-3.

Takagi, K., M. Nomura, D. Ashiya, H. Takahashi, K. Sasa, Y. Fujinuma, H. Shibata, Y. Akibayashi, and T. Koike (2005), Dynamic carbon dioxide exchange through snowpack by wind-driven mass transfer in a conifer-broadleaf mixed forest in northernmost Japan, *Global Biogeochem. Cycles*, *19*, GB2012, doi:10.1029/2004GB002272.

Takahashi, T., et al. (2009), Climatological mean and decadal change in surface ocean pCO_2, and net sea-air CO_2 flux over the global oceans, *Deep Sea Res., Part II*, *56*(8–10), 554–577, doi:10.1016/j.dsr2.2008.12.009.

Thomas, D. N., and G. S. Dieckmann (2002), Biogeochemistry of Antarctic sea ice, *Oceanogr. Mar. Biol.*, *40*, 143–169.

Timmermann, R., H. H. Hellmer, and A. Beckmann (2002), Simulations of ice-ocean dynamics in the Weddell Sea 2. Interannual variability 1985–1993, *J. Geophys. Res.*, *107*(C3), 11.11–11.19, doi:10.1029/2000JC000742.

Tison, J. L., C. Haas, M. M. Gowing, S. Sleewaegen, and A. Bernard (2002), Tank study of physico-chemical controls on gas content and composition during growth of young sea ice, *J. Glaciol.*, *48*(161), 177–191.

Tison, J. L., A. Worby, B. Delille, F. Brabant, S. Papadimitriou, D. Thomas, J. de Jong, D. Lannuzel, and C. Haas (2008), Temporal evolution of decaying summer first-year sea ice in the Western Weddell Sea, Antarctica, *Deep Sea Res., Part II*, *55*(8–9), 975–987, doi:10.1016/j.dsr2.2007.12.021.

Vancoppenolle, M., C. M. Bitz, and T. Fichefet (2007), Summer landfast sea ice desalination at Point Barrow, Alaska: Modeling and observations, *J. Geophys. Res.*, *112*, C04022, doi:10.1029/2006jc003493.

Vancoppenolle, M., T. Fichefet, H. Goosse, S. Bouillon, G. Madec, and M. A. M. Maqueda (2008), Simulating the mass balance and salinity of Arctic and Antarctic sea ice. 1. Model description and validation, *Ocean Model.*, *27*(1–2), 33–53, doi:10.1016/j.ocemod.2008.10.005.

Wadhams, P., M. A. Lange, and S. F. Ackley (1987), The ice thickness distribution across the Atlantic sector of the Antarctic ocean in midwinter, *J. Geophys. Res.*, *92*(C13), 14,535–14,552.

Weeks, W. F., and S. F. Ackley (1986), The growth, structure and properties of sea ice, in *The Growth, Structure and Properties of Sea Ice*, edited by N. Untersteiner, pp. 9–164, Plenum, N. Y.

Weiss, R. F. (1987), Winter Weddell Sea Project 1986: Trace gas studies during legs ANT V/2 and ANT V/3 of Polarstern, *Antarct. J. U. S.*, *22*, 99–100.

Weiss, R. F., H. G. Ostlund, and H. Craig (1979), Geochemical studies of the Weddell Sea, *Deep Sea Res., Part A*, *26*, 1093–1120, doi:10.1016/0198-0149(79)90059-1.

Wettlaufer, J. S., M. G. Worster, and H. E. Huppert (1997), Natural convection during solidification of an alloy from above with application to the evolution of sea ice, *J. Fluid Mech.*, *344*, 291–316, doi:10.1017/S0022112097006022.

Zemmelink, H. J., B. Delille, J. L. Tison, E. J. Hintsa, L. Houghton, and J. W. H. Dacey (2006), CO_2 deposition over the multi-year ice of the western Weddell Sea, *Geophys. Res. Lett.*, *33*, L13606, doi:10.1029/2006gl026320.

Zhou, J., B. Delille, H. Eicken, M. Vancoppenolle, F. Brabant, G. Carnat, N.-X. Geilfus, T. Papakyriakou, B. Heinesch, and J.-L. Tison (2013), Physical and biogeochemical properties in landfast sea ice (Barrow, Alaska): Insights on brine and gas dynamics across seasons, *J. Geophys. Res. Oceans*, *118*, 3172–3189, doi:10.1002/jgrc.20232.